Attenuation mechanism effect on filter shape in channelized dynamic spectral equalizers

Sang-Hyun Oh and Dan M. Marom

Free-space-based channelized dynamic spectral equalizers are theoretically investigated by solving the temporal-frequency-dependent power-coupling integral for commonly used active device technologies: liquid-crystal modulators, tilting micromirror arrays, and deformable gratings. Channel-filter characteristics, such as bandwidth and interchannel transition, are found to depend on the different attenuation mechanisms provided by the active devices. Such information is required for choosing the proper device parameters in designing channel equalizers and similar free-space spatially dispersed subsystems.

OCIS codes: 060.2340, 070.6110, 230.6120, 010.1080, 120.2440.

1. Introduction

Dynamic spectral equalizers (DSEs) are one of the newly emerging elements in optical networks, which are evolving toward greater transparency, longer reach, and reconfigurability. Because channel power disparity in dense-wavelength division multiplexed (DWDM) optical communication systems can lead to detection errors due to reduced optical signal-to-noise ratio and finite detector sensitivity,[1] DSEs have been deployed to flatten the gain profile of optical amplifiers. First-generation DSEs exhibited low spectral resolution because they were designed to match the slow variation of the amplifier's gain profile. Today's DWDM optical networks require optical add–drop capability as well as broadcast-and-select topologies.[1] Such capabilities are provided by high-resolution, channelized DSEs that provide wide, flat passbands for each wavelength channel and that can attenuate each channel independently to an extinction exceeding 30 dB. These requirements are necessary for cascading multiple DSEs in the signal path with minimal filtering impairments.

Several implementations of channelized DSEs are based on a dispersive, free-space imaging configuration,[2–4] that projects the light emerging from the input fiber via imaging lenses and a diffraction grating onto a pixelated device plane (Fig. 1). The dispersive imaging arrangement demultiplexes the input DWDM channels in space so that the information bandwidth of each wavelength channel is well contained within an active pixel element. The light is collected from the active modulating elements and is coupled into an output fiber after backpropagating through the dispersive arrangement (reversing the original spatial dispersion). Ensuring that the mode size on the device array plane is less than the active pixel width yields the desired wide passband characteristics. Furthermore, a wide spatial margin between the incident beam and the pixel edges results in guard bands, which allow for drift in the laser source, misalignment of the optical system, and provides a more abrupt interchannel transition. Thus the primary concern in the optical system design of a channelized DSE is that it provide sufficient spatial dispersion to contain the significant portion of the channel bandwidth within the pixel. This can be achieved by a judicious choice of the diffraction grating frequency and effective focal length of the imaging setup. However, the DSE filter shape also depends on the properties of the active modulating elements. The design of a channelized DSE, therefore, requires an understanding of these properties and of how to model the influence of the active attenuating element on the filter shape.

When this work was done, S.-H. Oh was with Agere Systems, Optical MEMS Research and Development, 4 Connell Drive, Berkeley Heights, New Jersey 07922. He is now with IBM Microelectronics Division, 2070 Route 52, Hopewell Junction, New York 12533. D. Marom (dmarom@lucent.com) is with Bell Laboratories, Lucent Technologies, 101 Crawfords Corner Road, Holmdel, New Jersey 07733.

Received 2 May 2003; revised manuscript received 16 September 2003; accepted 29 September 2003.

0003-6935/04/010127-05$15.00/0

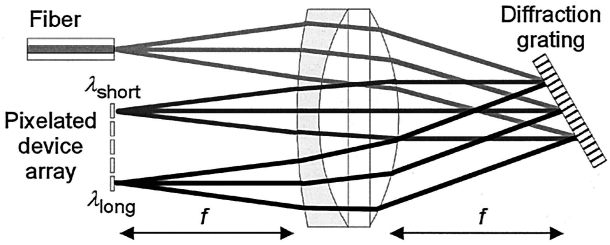

Fig. 1. One possible layout of a free-spaced-based channelized DSE. The fiber shown serves as both the input and output ports via a circulator (not shown).

2. System Modeling

The active pixelated device can be chosen from a variety of available technologies; however, liquid-crystal modulators[4] (LCMs), microelectromechanical-system (MEMS) tilting mirror arrays,[3] and deformable gratings[5] (referred to as diffractive MEMS or DMEMS) are often the technologies of choice. The loss mechanism of each of these technologies is different. MEMS tilting mirrors change the propagation direction of the reflected beams, which introduces a loss when coupling back to the output single-mode fiber. Furthermore, the tilt direction of the MEMS mirrors is an additional parameter that affects the filter shape. A mirror can tilt in the direction orthogonal to dispersion [DOD; Fig. 2(a)] or tilt in the dispersion direction [DD, Fig. 2(b)]. LCMs [Fig. 2(c)] attenuate the intensity of the light transmitted through the pixels by polarization rotation and extinction by means of a crossed polarizer (reflective designs are also possible, without loss of generality). DMEMS [Fig. 2(d)] consist of slender, periodic reflective ribbons with fill ratio of one half (ribbon width equal to gap width), suspended above a reflective plane such that reflectivity from the ribbons and the plane below are in phase. Changing the spacing between the ribbons and underlying plane yields destructive interference that serves to attenuate the reflected signal.

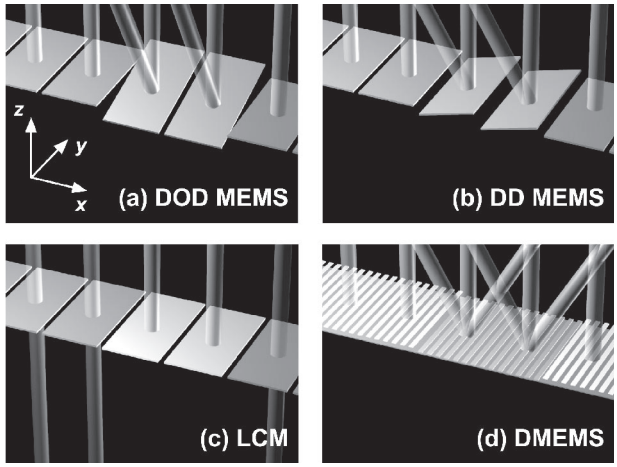

Fig. 2. Attenuation mechanisms of active devices: (a) MEMS mirrors with DOD tilt, (b) MEMS mirrors with DD tilt, (c) LCM, (d) DMEMS.

The channel filter shape is calculated by solving the power-coupling efficiency integral as a function of the signal frequency. The ideal Gaussian beam model is used, whereas imaging system aberrations and clipping (vignetting) by the system's apertures are ignored. The Gaussian mode, spatially dispersed in the x direction and with normalized power, is given by

$$\psi_{\text{input}}(x, y, f) = \left(\frac{2}{\pi\omega_{0x}\omega_{0y}}\right)^{1/2} \exp\left[-\frac{(x - pf/f_0)^2}{\omega_{0x}^2} - \frac{y^2}{\omega_{0y}^2}\right], \tag{1}$$

where x and y are the transverse spatial coordinates, ω_{0x} and ω_{0y} are the mode field radii at the device plane in the x- and y-axis directions, respectively (Gaussian waist assumed on device plane), p is the pitch or center-to-center distance between adjacent pixels, f_0 is the channel spacing of the DWDM system (in hertz), and f is the temporal frequency (also in hertz). Equation (1) allows for elliptical Gaussian modes (independent widths in the x and y directions) as a consequence of spatial mode projection in the grating diffraction process that generates an anamorphic effect. The term pf/f_0 defines the center location of the Gaussian mode as a function of frequency, owing to the spatial dispersion of the imaging system, where the spatial dispersion is assumed to be constant over the operating band. In practice, however, the dispersion is not constant owing to the wavelength dependence of the grating diffraction angle. Note that only the ratio p/ω_{0x} determines the passband performance; thus the designer can vary the spot size and then adjust the amount of spatial dispersion to maintain identical performance. The Gaussian beam imaged onto the active device array plane may be well contained within a single pixel for the WDM channel frequencies or be divided over two adjacent pixels. In the latter case, the two independently modulated beam portions are combined at the output fiber (image plane of the active device), neglecting the imaging system's finite modulation transfer function, and coupled back to the fiber (the power-coupling efficiency is obtained by performing the traditional overlap integral[6]). The general form of the modulated field, by use of the Kirchhoff approximation, is given by

$$\psi_{\text{output}}(x, y, f) = \psi_{\text{input}}(x, y, f) \times \sum_{n=0}^{N-1} A_n \exp[i(kx \sin\theta_{x,n} + ky \sin\theta_{y,n} + \varphi_n)]\text{rect}\left(\frac{x - np}{p}\right). \tag{2}$$

The pixelated active array is modeled by the finite sum (N pixels for corresponding N DWDM channels),

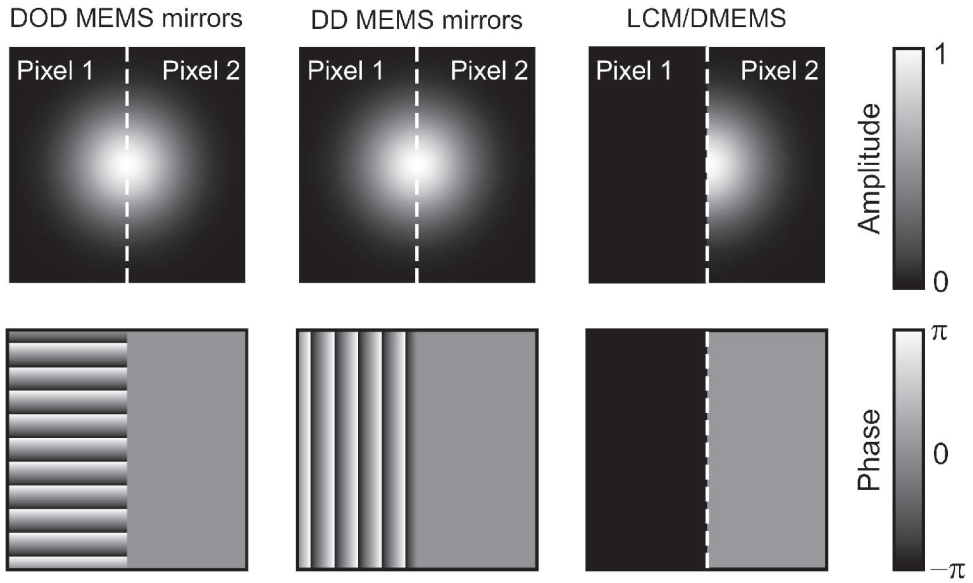

Fig. 3. Amplitude and phase of a modulated output beam for MEMS mirrors with DOD tilt (left-hand side), DD tilt (middle), and LCM and DMEMS devices (right-hand side). Pixel 1 at 35 dB attenuation mode; pixel 2 no attenuation.

where the nth pixel has an amplitude attenuation coefficient A_n, an x-direction propagation component $\theta_{x,n}$, a y-direction propagation component $\theta_{y,n}$, and finite spatial extent corresponding to the pixel width p adjusted to the proper pixel location (the N pixels are contiguous). This model uses the notation that the N DWDM channels are at frequencies $f = nf_0$, for $n = 0, \ldots, N - 1$. Thus the input Gaussian mode, with its infinite extent in the spatial domain, is theoretically affected by all the pixels in the device array. However, owing to the desired condition that $p > \omega_{0x}$ (to achieve the wide passbands), only the neighboring pixels have a perceptible effect. MEMS mirrors with DOD tilt are modeled by setting all $A_n = 1$ and $\theta_{x,n} = 0$, with each pixel generating a unique beam propagation direction $\theta_{y,n}$ that is twice the mirror tilt angle setting. Similarly, in the case of MEMS mirrors with DD tilt, all $A_n = 1$ and $\theta_{y,n} = 0$, and each mirror gives rise to a unique beam propagation direction $\theta_{x,n}$. Additionally, for both MEMS mirror tilt directions, there is a phase constant φ_n that is associated with mirror sag. This constant accounts for the fact that the mirror is suspended from spring elements and that, in addition to the desired rotation, the electrostatic force causes mirror displacement toward the electrodes. This sag varies the relative phase relationship between neighboring mirrors. In the case of the LCM attenuator, the beam propagation directions do not change ($\theta_{x,n} = \theta_{y,n} = 0$). However, each pixel is set to a unique field attenuation setting A_n, which is coupled to an associated absolute phase delay φ_n (the complex LCM transfer function, determined by Jones matrix modeling of the LCM's response, is given by $[1 + \exp(-j\varphi)]/2$). DMEMS devices theoretically excite infinite diffraction orders, where the power in each order is determined by the distance (or phase delay) between the ribbons and the underlying plane. However, only the zeroth order (reflected signal) is allowed to propagate to the output fiber. The zeroth order has a complex reflection coefficient of $[1 + \exp(-j\varphi)]/2$, where φ is the phase delay between adjacent ribbons, which implies that its physical response is identical to that of the LCM. Figure 3 illustrates the output field (amplitude and phase) for a Gaussian beam at a frequency midway between two WDM channels (thus striking two active elements) for the investigated device options when one pixel is set for high attenuation.

3. Modeling Results

In this study the channel pitch (measured as a spatial width) is set to 2.75 times the Gaussian field diameter ($2\omega_{0x}$) on the device plane, and the channels are on a $f_0 = 100$-GHz spacing. For convenience the overlap integral can be evaluated on the device plane between the modulated field (Eq. [2]) and the image of the output fiber onto the device plane.[6] Note that the backpropagation of the output fiber mode results in the same field distribution as the original input field defined by Eq. (1). The frequency-dependent coupling efficiency integral

$$\eta(f) = \left| \int \psi_{\text{input}}(x, y, f)\psi_{\text{output}}(x, y, f)\mathrm{d}x\mathrm{d}y \right|^2$$

can be evaluated for any active device technology and setting, provided that the proper coefficients are chosen to model the MEMS mirror devices with DD or DOD tilts or with the LCM/DMEMS devices in ψ_{output}. The channel-filtering effects are explored for the following three cases: (1) adjacent channels are both transmitting, (2) adjacent channels are both attenuating (to the 5-, 10-, and 35-dB transmission levels), and (3) one channel is fully transmitting while the other is attenuating. The four-channel sequence of "transmit," "transmit," "attenuate," and

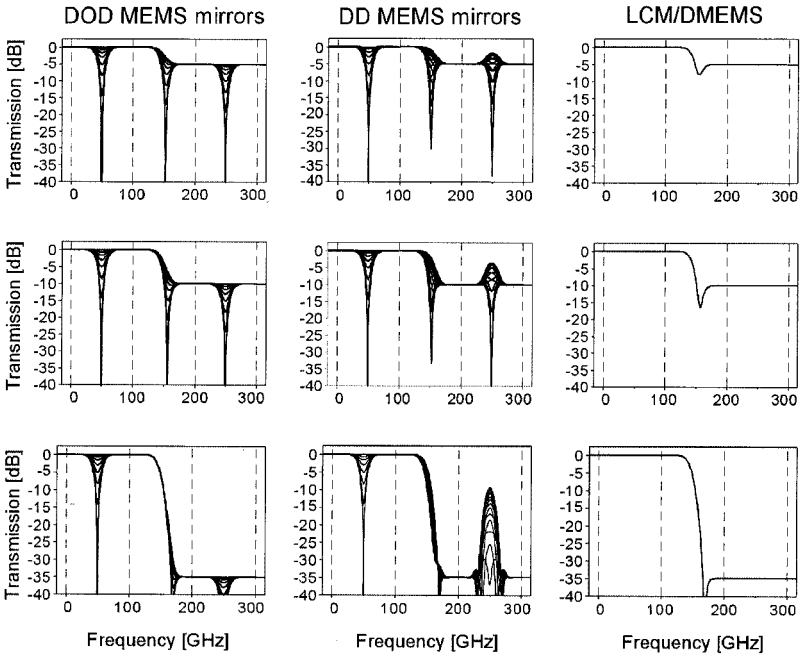

Fig. 4. Calculated filter shapes for different active pixel technologies applied to four channels in a "transmit," "transmit," "attenuate," and "attenuate" pattern. Attenuation set at −5 dB (top row), −10 dB (center row), and −35 dB (bottom row).

"attenuate" encompasses these three cases and is plotted for the different device options (Fig. 4). For each MEMS mirror type, a family of curves is shown where the relative phase between neighboring mirrors is varied from 0 to 2π. This serves to model the effect of the MEMS mirror sag. The actual phase is a function of the mirror geometry, spring design, voltage applied to the electrodes, and fabrication uniformity. The relative phase between adjacent MEMS mirrors has a large effect on the interchannel transition band structure, especially for mirrors with DD tilt due to the abrupt phase jump across the gap. At the transition band, the Gaussian mode illuminates two adjacent mirrors, with the relative phases contributing either constructively (in phase) or destructively (out of phase) to the fiber coupling integral. The mirror with DD tilt exhibits significant coupling at the interchannel transition position in attenuation mode. This is due to the diffraction from the mirror's edge that excites an angular bandwidth that couples back to the output fiber. When the mirror is tilted with DOD, this same angular bandwidth is also tilted away from the output fiber acceptance angle. Passband widths measured within a ±3-dB range at an attenuation level between 0 and 10 dB, as well as stopband widths measured at the 30-dB attenuation levels, are used for comparison, with the worst case chosen from the family of relative phase curves). The passband width is 73 GHz for DOD MEMS mirrors, 74 GHz for DD tilt, and 76 GHz for the LCM/DMEMS device. The stopband width of the attenuated channel, which is important for cross-talk suppression, is 60 GHz for DOD MEMS mirrors, 66 GHz for DD tilt, and 71 GHz for the LCM/DMEMS device.

In practice, both the MEMS and LCM devices require that a finite gap exist between adjacent pixels. In the case of tilting MEMS mirrors, the beam incident on the gap is not reflected back to the optical system and is thus completely lost. With the LCM, however, two options are available: transparent gap, in which the fraction of the beam incident on the gap is transmitted, or opaque gap, which absorbs the light. The effect of a finite, nonreflecting gap is modeled by decreasing the size of the active pixel in Eq. (2) by setting the denominator of the rect function to p-gap. A transparent gap is modeled by the addition of the component of light incident on the gap. We choose to ignore the effect of fringing fields for the transparent gap case, which can be modeled by finite penetration into the gap region, effectively reducing the gap width. The gap is chosen to be one fifth of the Gaussian waist diameter on the device plane. In the case of the LCM, two curves are plotted for opaque and transparent pixel gaps (Fig. 5). Interchannel coupling is also evident in the LCM with transparent gaps. The passband width for DOD MEMS mirrors is 75 GHz; DD tilt, 75 GHz; LCM with opaque gap, 77 GHz; and LCM with a transparent gap, 68 GHz. Corresponding stopband widths are 68, 63, 77, and 63 GHz, respectively.

4. Conclusions

The filter-shape dependence on the attenuation mechanism in channelized DSEs that use tilting MEMS mirrors, LCMs, or DMEMS devices has been investigated by use of a model based on the calculation of the fiber coupling integral that provides a basis for optimized system design. The findings show that the attenuation mechanism provided by

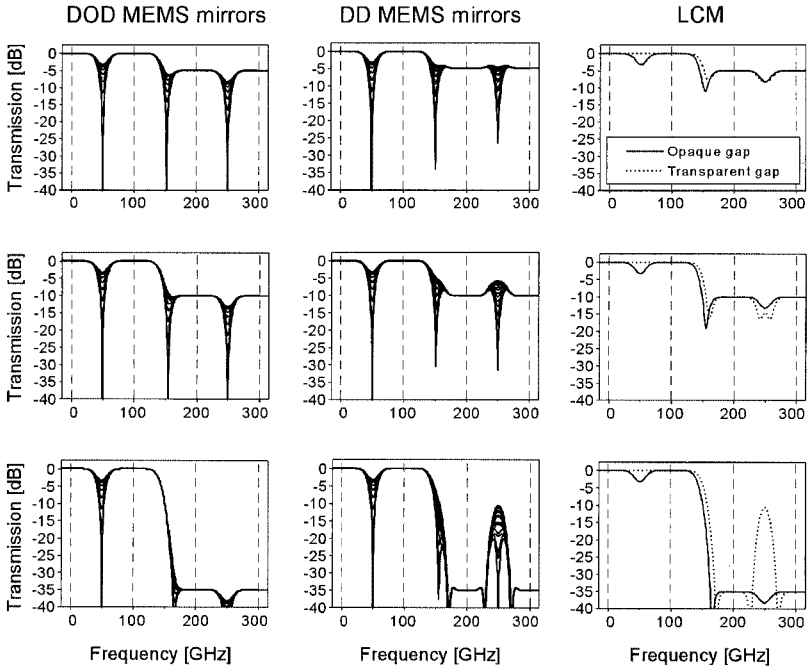

Fig. 5. Channel-filter characteristics as in Fig. 4, including gaps between active elements. For LCM, both opaque and transparent gaps are shown.

DMEMS and LCM devices with opaque gaps yields the widest passbands and stopbands, which are desirable system attributes. MEMS mirrors with DOD tilt are preferable over mirrors with DD tilt because the diffraction from the DOD tilt mirror's edge does not couple back to the fiber in attenuated mode (i.e., reduce the stopband width), and they offer smoother interchannel transitions that lead to wider passbands. The complex interchannel transition structure of the mirrors with DD tilt is attributed to the abrupt phase jump across the pixel boundary, whereas for DOD tilt mirrors the phase varies along the pixel boundary and its effect is averaged in integration (see Fig. 3). By designing MEMS mirrors with DOD tilt and minimal sag (such that phase variations between mirrors is small), one can match their channel filter shape characteristic to that of the LCM devices (see Fig. 5). Consequently, such low-sag, DOD tilt, MEMS mirrors provide the greatest functionality because they offer wide passband and stopband widths, easily achieve high extinction ratios, and are expandable to higher output port count subsystems.[7,8]

References

1. T. E. Stern and K. Bala, *Multiwavelength Optical Networks* (Addison-Wesley, Reading, Mass., 1999), Chap. 4.
2. J. E. Ford and J. A. Walker, "Dynamic spectral power equalization using micro-optomechanics," IEEE Photon. Technol. Lett. **10,** 1440–42 (1998).
3. D. T. Neilson, D. S. Greywall, S. Chandrasekhar, L. L. Buhl, H. Tang, L. Ko, N. R. Basavanhally, F. Pardo, D. A. Ramsey, J. D. Weld, Y. L. Low, J. Prybyla, R. Scotti, A. Gasparyan, M. Haueis, S. Arney, S. P. O'Neill, C.-S. Pai, D. H. Malkani, M. M. Meyers, N. Saluzzi, S.-H. Oh, O. D. Lopez, G. R. Bogart, F. P. Klemens, M. Luo, J. Q. Liu, K. Teffeau, A. Ramirez, K. S. Werder, J. E. Griffith, C. Frye, M. V. Kunnavakkam, S. T. Stanton, J. A. Liddle, H. T. Soh, T.-C. Lee, O. Nalamasu, and K. C. Nguyen, "High-dynamic range channelized MEMS equalizing filter," in *Digest of Optical Fiber Communication Conference* (Optical Society of America, Washington, D.C., 2002), p. 586.
4. J. Kondis, B. A. Scott, A. Ranalli, and R. Lindquist, "Liquid crystals in bulk optics-based DWDM optical switches and spectral equalizers," in *2001 IEEE LEOS Annual Meeting* (Institute of Electrical and Electronics Engineers, New York, 2001), Vol. 1, pp. 292–293.
5. O. Solgaard, F. S. A. Sandejas, and D. M. Bloom, "Deformable grating optical modulator," Opt. Lett. **17,** 688–690 (1992).
6. R. E. Wagner and W. J. Tomlinson, "Coupling efficiency of optics in single-mode fiber components," Appl. Opt. **21,** 2671–2688 (1982).
7. J. E. Ford, V. A. Aksyuk, D. J. Bishop, and J. A. Walker, "Wavelength add–drop switching using tilting micromirrors," IEEE J. Lightwave Technol. **17,** 904–911 (1999).
8. D. M. Marom, D. T. Neilson, D. S. Greywall, N. R. Basavanhally, P. R. Kolodner, Y. L. Low, F. Pardo, C. A. Bolle, S. Chandrasekhar, L. Buhl, C. R. Giles, S.-H. Oh, C. S. Pai, K. Werder, H. T. Soh, G. R. Bogart, E. Ferry, F. P. Klemens, K. Teffeau, J. F. Miner, S. Rogers, J. E. Bower, R. C. Keller, and W. Mansfield, "Wavelength-selective 1 × 4 Switch for 128 WDM channels at 50 GHz spacing," in *Digest of Optical Fiber Communication Conference* (Optical Society of America, Washington, D.C., 2002), postdeadline paper FB-7.